EUROPEAN ORGANIZATION FOR NUCLEAR RESEARCH

CERN-EP/99-165
19 November 1999

Gross properties of exotic nuclei investigated at storage rings and ion traps *

C. Scheidenberger[1,2], G. Bollen[3,2], F. Bosch[1], A. Casares[4], H. Geissel[1,4], A. Kholomeev[4], G. Münzenberg[1,5], H. Weick[4,1], H. Wollnik[4],

[1] *GSI, D-64291 Darmstadt*
[2] *CERN, CH-1211 Geneva 23*
[3] *Ludwig-Maximilians-Universität, D-85748 München*
[4] *Justus-Liebig-Universität Gießen, D-35392 Gießen*
[5] *Johannes Gutenberg-Universität Mainz, D-55099 Mainz*

Abstract. Properties of exotic nuclei like atomic masses, decay modes, and half-lives can be ideally investigated in storage rings and ion traps. Some experiments can be carried out under conditions which prevail in hot stellar plasmas. The experimental potential of storage and cooling of exotic nuclei is illustrated with recent experimental results and an outlook to future experiments is presented.

ISOLDE GENERAL

*) Invited talk at the 4th International Conference on Physics at Storage Rings STORI'99, Bloomington, Indiana U.S.A., 12-16. Sept. 1999

INTRODUCTION

Beams of exotic heavy nuclei and of antiprotons are used for a large variety of investigations in physics ranging from the test of fundamental symmetries and physical constants [1,2] to structure studies of complex nuclei [3–5]. The common feature of these experiments is that the particles under investigation are not available from conventional ion sources but have to be produced in dedicated nuclear reactions [1,4,6]. Therefore, it was necessary to develop techniques and devices for production, separation, accumulation, bunching, storage, and cooling of the reaction products: electromagnetic separators, storage rings, and ion traps [7].
In the first part of this paper the concepts and experimental techniques for production and handling of exotic nuclear beams in ion traps and storage rings are outlined. The characteristic features of the production mechanisms fusion, fragmentation, spallation, and fission are briefly described together with the two basic separation concepts ISOL (Isotope Separation On-Line) and in-flight separation. The second part concentrates on precision mass measurements of exotic nuclei at ISOLDE (CERN) and SIS-FRS-ESR (GSI). The third part highlights a new class of experiments which became possible in the experimental storage ring ESR with ions which can be called 'exotic' because of their high charge state: manipulation of the nuclear lifetimes in dependence of their ionic charge state of bare and few-electron heavy ions. Finally new ideas for sub-millisecond direct mass measurements of fusion-reaction products at SHIP and of projectile or fission fragments at the FRS are presented and an outlook to new applications is given.

THE EXPERIMENTAL TECHNIQUES

Sources of exotic nuclei

Antiprotons are produced in collisions of intense proton beams with heavy target materials like copper or iridium. Due to energy and momentum conservation the laboratory threshold energy amounts to six times the proton rest mass and the optimum yield lies around 26GeV/c. For the production of exotic heavy nuclei there are basically three methods available: 1) proton- or neutron-induced target fragmentation (spallation) or fission, 2) projectile fragmentation or fission, and 3) heavy ion fusion. While the first method is usually related to ISOL devices [6] the latter two yield energetic reaction products which can be separated in-flight with recoil separators and fragment separators [8].
The statistical nature of projectile fragmentation leads to the formation of a large variety of ion species, in particular exotic nuclei with unusual proton-to-neutron ratios, which predominately populate the area between the stable isotopes and the proton dripline ranging from the projectile atomic number down to the lightest elements. Target spallation, where the fragmentation reactions are induced by a light ion beam (protons, neutrons or light ions), can be described in a similar way [4].

Electromagnetic dissociation (ED) mainly takes place in collisions with high-Z target nuclei and leads to the evaporation of neutrons and/or (in the case of heavy projectiles like lead or uranium) to projectile fission. At an ISOL system the role of projectile and target is reversed and the heavy target nuclei fission after proton bombardment. In both cases predominantly neutron-rich fission fragments are produced because the fission event mostly takes place after excitation of the giant dipole resonance ($\sim$10MeV) thus leading to cold fission. Heavy ion fusion reactions take place at projectile energies just sufficient to cross the Coulomb barrier, which is of the order of 5MeV/u. The projectile and target nucleus merge to a compound nucleus, which de-excites evaporating nucleons, the number of which depends on the excitation energy.

Separation, accumulation, storage, and cooling of exotic nuclei with storage rings and ion traps

In-flight separated and short-lived heavy ion fusion products can be investigated at the GSI velocity filter SHIP [9] and at the gas-filled separator NASE [10]. In this low-energy domain the heavy recoils carry many electrons and are distributed over many different ionic charge states with typical abundances of the order of 10% each [11]. To obtain a high collection efficiency and transmission the many different charge states are 'focused' in gas-filled separators on an average charge state $\overline{q} \simeq (v/v_0) \cdot Z^{1/3}$ [12].
At the high-energy heavy-ion facilities SIS-FRS-ESR relativistic exotic nuclei are generated in a production target placed at the entrance of the fragment separator FRS [13]. At relativistic velocities the ions emerge from the production target mainly as bare or few-electron projectiles [14]. Two separation schemes are applicable at the FRS: pure magnetic $B\rho$-analysis and a combined $B\rho$–ΔE–$B\rho$-analysis. In the first case all fragments with the same magnetic rigidity $B\rho$ are transmitted within an acceptance of $\Delta B\rho/(B\rho) \simeq \pm 1$ % and a multi-component 'cocktail beam' can be injected into the storage ring ESR [15]. In the second case the FRS is operated as momentum-loss achromat and an energy degrader is placed in the dispersive midplane. This mode is used either when it is necessary to reduce the number of different species in cocktail beams and/or to suppress high-intensity beam components or when an experiment requires monoisotopic secondary beams. Figure 1 illustrates both scenarios showing the spectra of stored cooled Ni fragments using pure $B\rho$ analysis (left spectrum) and using $B\rho$–ΔE–$B\rho$-separation of bare ^{52}Mn (right spectrum), respectively [16].
The shown spectra have been obtained with Schottky noise diagnosis and FFT frequency analysis [17,18]. The area of each peak, the noise power, is proportional to the number of stored ions. The sensitivity of this method is so high, that even single ions [19] can be detected and their revolution frequency can be determined. Therefore, Schottky diagnosis is well suited for experiments with stored exotic secondary beams, where only low intensities are available due to the small production cross sections. The width of the frequency peaks is proportional to the relative longitudinal velocity spread $\delta v/v$ and therefore efficient cooling is required for high frequency

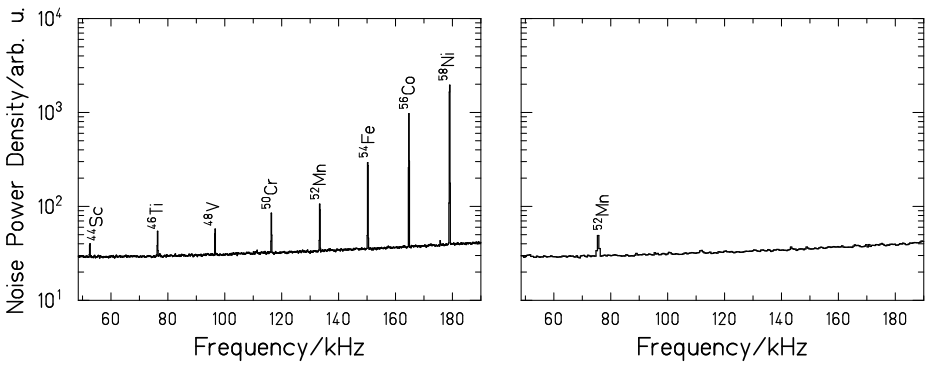

FIGURE 1. Schottky noise power spectra of cooled bare Ni fragments stored in the ESR [16]. **Left panel:** pure $B\rho$ analysis was applied and thus many different bare fragments with similar m/q are transmitted through the FRS. **Right panel:** by the use of an intermediate degrader the combined $B\rho$–ΔE–$B\rho$-analysis was applied leading to a monoisotopic secondary beam; the FRS was tuned for separation of $^{52}Mn^{25+}$.

and mass resolution of multicomponent beams (see below). For precooling of the hot fragments stochastic Palmer cooling is available [20], which reduces the phase space down to $\delta p/p = \pm 0.1$ %. With electron cooling [21,22] the longitudinal momentum spread can be further reduced down to $\delta p/p \leq 1 \cdot 10^{-6}$ for stored beams containing less than a few thousand ions [21].

At ISOLDE the exotic nuclei produced and stopped in the thick production target [23] are released from the target, ionized, and are then separated with electromagnetic separators, the general purpose separator GPS and the high-resolution separator HRS, respectively. The secondary ion yields at ISOL-type facilities are not only determined by the product of driver beam intensity, target thickness and production cross section but also, and sometimes even more crucial are diffusion and release processes from the target, transfer efficiencies to the ion source, ionization probabilities and finally radioactive decay during the entire process [6]. With respect to the individual physical and chemical properties and peculiarities a large variety of target–transfer-line–ion-source–combinations has been developed in more than 30 years [6] to meet the specific experimental requirements like high secondary beam intensities, few or even no isobaric contaminants, element selectivity, and short half-lives. Presently beams of 70% of the chemical elements can be provided and the nuclei with the shortest half-lives are ^{14}Be ($T_{1/2} = 4.4$ms) and ^{11}Li ($T_{1/2} = 8.5$ms). The ions are usually singly ionized and typical ion beam emittances are of the order of 30π mm mrad at 60keV beam energy.

Several schemes for ion-beam accumulation, cooling, and bunching in ion traps have been developed [24]. At the ISOLTRAP experiment [25,26] a Penning trap was used as an accumulator, cooler, and buncher for the low-energy (typically 30keV or 60keV) secondary beams at ISOLDE [27,28]. This cooler trap is a segmented linear Penning trap with cylindrical electrodes, filled with He buffer gas with a pressure $\sim 10^{-5} \ldots 10^{-4}$mbar. To the various segments different voltages are applied for the formation of a longitudinal potential well for the ions as shown in figure 2 [28]. The height of the potential step at the entrance of the trap is attuned to the kinetic

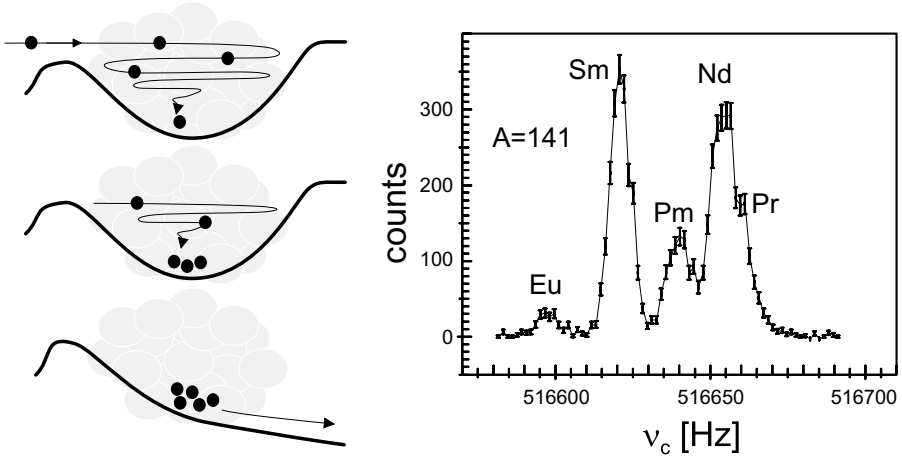

FIGURE 2. Left: Principle of continuous accumulation, buffer gas cooling, and bunching of ions in a cooler trap [28]. **Right:** This mass scan for $A = 141$-isobar shows the number of ejected ions as a function of the rf-frequency after mass-selective cooling [28].

energy of the injected ions so that they can pass this barrier once at their arrival. Then, the ions loose kinetic (and thus potential) energy in collisions with the buffer gas atoms and are slowed down until they are thermalized in the central potential well of the trap: the longitudinal ion motion has been cooled and an ion bunch was formed. For the transverse motion the dissipation of energy leads to an increase of the magnetron motion amplitude. This instability can be avoided for ions with mass-to-charge ratio m/q when an azimuthal rf-field with a frequency equal to the cyclotron frequency $\omega_c = q/m \cdot B$ is applied [29]. Ions with the proper m/q-ratio are centered in the trap whereas other ions are lost. Hence, this process is mass selective and can be used for mass separation. This scheme for capture, cooling, bunching, and separation of secondary beams has been pioneered at ISOLTRAP and will be used at the radioactive beam experiment REX-ISOLDE [30] and at the SHIPTRAP [31] project.

Facilities combining storage rings and ion traps

New precision experiments will become possible with ion traps capturing decelerated beams extracted from storage rings, for instance at the antiproton decelerator AD [1] at CERN or at the heavy ion trap experiment HITRAP [32] downstream of the ESR. In the latter experiment the ESR is used for accumulation and subsequent deceleration of highly or even fully stripped heavy ions from primary or secondary beams down to specific kinetic energies of the order of few MeV/u. After extraction and further deceleration the highly-charged ions will be captured in a Penning trap for experiments. Among other experiments like accurate mass measurements of stable and unstable isotopes, the main interest will be devoted to g-factor measurements of the bound electron in heavy one-electron ions, which is a sensitive test for QED [33]. Systematic hyperfine-structure investigations in isotopic chains will yield new insights on details of the magnetic moments and structure of nuclei.

The ATHENA [34] and the ATRAP [35] experiments at the AD are aiming at the capture of decelerated antiprotons and of positrons for the production and study of cold antihydrogen. In view of testing CPT-invariance these experiments focus on high-precision comparisons of matter and antimatter properties like inertial masses and atomic energy levels and transitions. So far the proton and antiproton masses agree within $9 \cdot 10^{-11}$ [36].

EXPERIMENTS AND RESULTS

Direct mass measurements

In this chapter some experiments on direct mass measurements of short-lived nuclei are presented. For recent reviews covering also other techniques the reader is referred to [37,38]. The motivation for accurate mass measurements is manyfold and the field has attracted lively interest over many decades. There are whole regions which are subject of general interest in the study of nuclear structure and effects as indicated in figure 3 and there are single isotopes whose masses are of particular interest, like for instance ^{32}Ar (see below).

Accurate mass measurements yield important information on nuclear structure and stability. The fundamental question: 'where are the limits of stability of nuclei' can be addressed in terms of the experimental determination of the drip line for neutrons and protons. Experiments exploring new regions of the chart of nuclei will possibly allow the discovery of new phenomena like new deformations, new regions of collectivity, and new interactions [39]. Some examples of present interest are briefly mentioned:

- nuclear binding energies and proton- and neutron-separation energies are key parameters for the study of skin and halo nuclei
- the existence of Thomas-Ehrman [40–42] shift in heavy nuclei
- proton-neutron pairing [39] and Wigner's SU(4) symmetry [43] can be studied in heavy $N = Z$ nuclei [44]
- study of deformation and shape-coexistence phenomena in the neutron-deficient region around the $Z = 82$ shell
- nuclear properties in the area around ^{208}Pb are important for the adjustment of nuclear-model parameters because it serves as a 'test ground' for the superheavy elements.
- Shell effects far off stability and shell quenching occurring in extremely neutron-rich nuclei have large impact on astrophysical theories modeling the paths of nucleosynthesis in stellar environments and the abundances of heavy nuclei

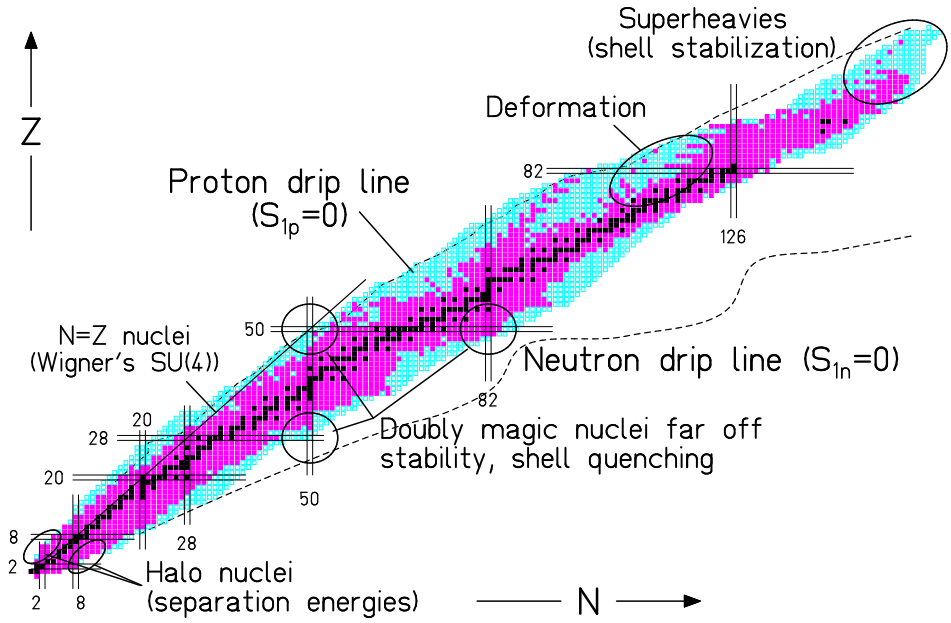

FIGURE 3. Schematic view of the chart of nuclei. Stable isotopes are indicated in black, known and unknown masses [45] in dark and light gray, respectively. Those candidates and areas which are of particular interest for mass measurements are indicated.

High-accuracy mass determinations with ISOLTRAP

The tandem Penning trap mass spectrometer ISOLTRAP [25,26] allows mass determinations of exotic nuclei with high accuracy. The setup consists of three main parts, a gas-filled rf-quadrupole for capture, cooling, and bunching of the ISOLDE beam, a linear cooler Penning trap for further cooling and for separation of isobaric contaminations (see above), and a hyperbolic high-precision Penning trap for mass measurements. The mass determination in the trap is based on the determination of the cyclotron frequency ω_c of the ion in a magnetic field of strength B according to $\omega_c = \omega_+ + \omega_- = B \cdot q/m$. The eigenmotions ω_+ and ω_- can be excited with dipole fields and the sum or difference of eigenfrequencies can be excited with a quadrupole field. At ISOLTRAP the sum $\omega_+ + \omega_-$ is excited by an azimuthal quadrupole field for the determination of the true cyclotron frequency ω_c. Due to the excitation the ions gain radial energy which is converted into axial energy when they pass through the inhomogeneous fringe field of the magnetic field at ejection. The measurement of the drift time to reach the detector as a function of the applied radio frequency yields a resonance curve with a characteristic minimum at ω_c. The magnetic field strength B is calibrated with ions of accurately known masses or, in other words, the unknown mass is obtained from the ratio of cyclotron frequency of the reference ion and that of the ion under investigation.

Under ideal conditions the achievable mass resolving power depends only on the excitation time T_{rf} and the Fourier-limited line width is $\Delta\nu_c(\mathrm{FWHM}) = 0.9/\mathrm{T_{rf}}$. A mass-resolving power $m/\Delta m(\mathrm{FWHM}) = 8 \cdot 10^6$ has been reached for $A = 133$ ions and for barium and caesium nuclei a mass accuracy of $\delta m/m \simeq 1 \cdot 10^{-7}$ is typically achieved for ions in the same mass range, corresponding to $\delta m \simeq 14\mathrm{keV}$ [46]. The

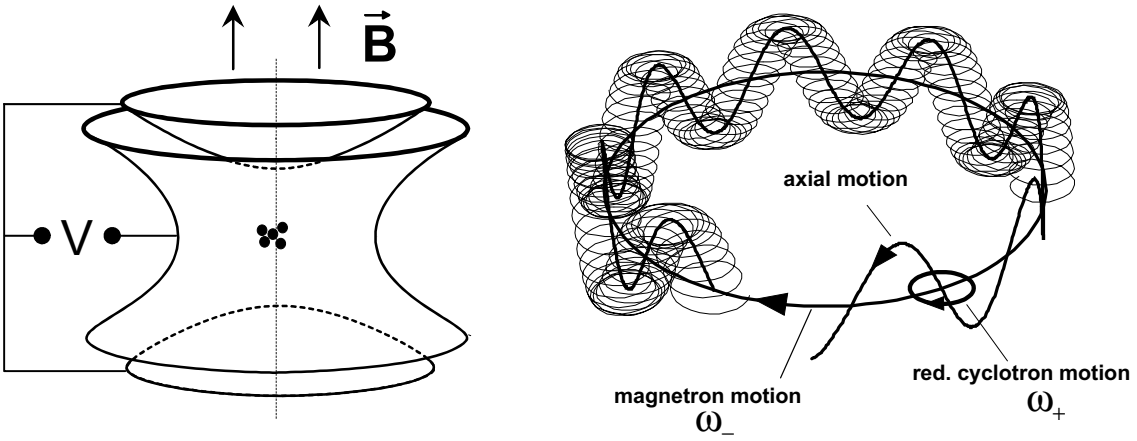

FIGURE 4. Left: Schematic drawing of the hyperbolic high-precision Penning trap for mass measurements. The magnetic field and the applied rf-voltage are indicated. **Right:** Schematic view of the three eigenmotions of an ion in a Penning trap [26].

experimental results will be discussed below.
In a recent experiment by Adelberger and co-workers [47] the (possible) weak scalar interaction is probed by studying positron-neutrino correlations in the pure Fermi transition of ^{32}Ar (for further reading see [48]). In this $0^+ \rightarrow 0^+$ β-decay the positron-neutrino correlation is derived from the energy spectrum of the delayed protons, which reflects the recoil momentum of the daughter nucleus of the super-allowed decay. With the results one can set constraints on the possible existence of scalar weak interactions. The result of the experiment is consistent with the Standard Model [47] but the analysis contains a systematic uncertainty which is due to the mass uncertainty of $\pm$50keV in ^{32}Ar. The authors used the isospin-multiplett mass equation [49] to obtain a more precise estimate. This result can be put on much safer ground with direct mass measurements which are accurate to $\simeq$ 5keV. It is now planned to determine the atomic mass of ^{32}Ar, which has a half-life of only 98ms, with this accuracy with the ISOLTRAP setup.

Mass determinations of very short-lived ions with MISTRAL and with Isochronous Mass Spectrometry (IMS)

The challenge in direct mass measurements of exotic nuclei is to develop experimental techniques which on the one hand allow accurate mass determination and on the other hand are fast in order to access nuclei far from stability which mostly have lifetimes much shorter than one second. These requirements are met by in-flight techniques as employed at MISTRAL (Mass measurements at ISolde using a Transmission RAdiofrequency spectrometer on-Line) [50] or with isochronous mass spectrometry IMS at the ESR [51].
In the MISTRAL experiment it is again the cyclotron frequency of the ion under investigation which is to be determined, here by means of two successive modulations of the kinetic energy while two revolutions in a Smith-type radiofrequency

spectrometer [52,53]. Ions for which the net effect of the radiofrequency modulation and demodulation vanishes are transmitted through the slit system (see figure 5) according to the condition

$$\omega_{\mathrm{rf}} = (n + 1/2) \cdot \omega_c \tag{1}$$

where n is an integer harmonic. The mass-resolving power of the instrument is proportional to n and inversely proportional to the width of the slit. Therefore, beam cooling is essential for a high transmission which is particularly important for experiments with low-intensity beams. The radiofrequency is scanned resulting in spectra as shown in the upper left part of figure 5 and the unknown masses are determined from a reference mass from the ratio of their measured cyclotron frequencies. An relative mass accuracy on the $8 \cdot 10^{-7}$-level is reached for nuclei around $A = 30$ [54,55].

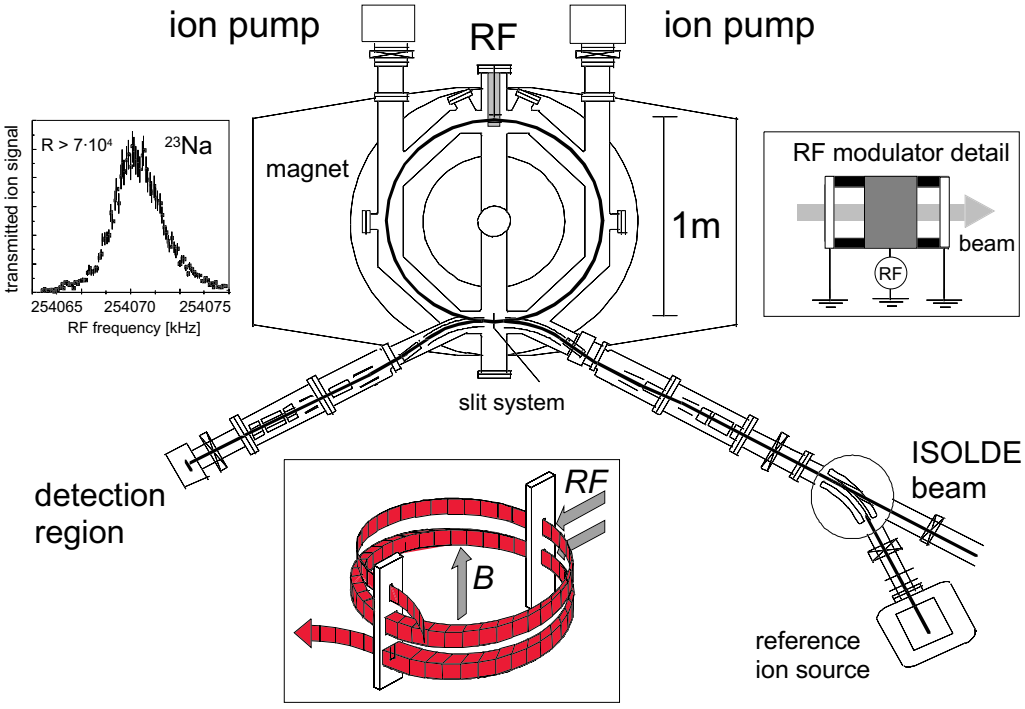

FIGURE 5. Schematic view of MISTRAL [50] showing the injection beam line, where ions delivered from ISOLDE are alternately injected with reference ions from an internal source, the spectrometer, and the detection region. The insets show the signal of a ^{23}Na beam transmitted through the spectrometer as a function of the modulation frequency (top left), the detail of the rf-modulator (top right), and the view of the trajectory envelope (center).

In recent experiments the masses of $^{23\ldots30}$Na isotopes have been determined, ^{28}Na having a half-life as short as 30.5ms [54]. The achieved mass accuracy was typically 20keV and the resolving power (FWHM) was in the vicinity of $1 \cdot 10^5$. In addition, atomic mass measurements of the elements ranging from Ne to Al have been performed [55] in order to investigate the region of the $N = 20$-shell closure in more detail [5]. This shell closure is located far from stability and for Ne the neutron

dripline comes close (see figure 3). Irregularities of the trends of two-neutron separation energies might be an indication for vanishing shells far from stability but there are also experimental hints for deformation effects [5].

Another approach for fast direct mass measurements are spectrometers with an isochronous ion optical characteristics like the TOFI spectrometer [56]. The time-of-flight of an ion through such a spectrometer is to first order independent of it's velocity and depends only on it's mass-to-charge ratio. The ESR when operated in an isochronous mode can be used as a multi-turn time-of-flight mass spectrometer [51,57], if the ions are injected with velocities v such that their Lorentz factor γ matches the ion-optical parameter $\gamma_{\rm tr}$ which characterizes the transition point of the storage ring. In this case ions with identical m/q have identical revolution times T because their velocity differences are compensated by appropriate flightpath differences [51]. From the equation for the mass-resolving power

$$\frac{\Delta(m/q)}{m/q} = \gamma_{\rm tr}^2 \cdot \frac{\Delta T}{T} + (\gamma_{\rm tr}^2 - \gamma^2) \cdot \frac{\Delta v}{v} \qquad (2)$$

one can easily see that $\Delta T/T$ becomes a direct measure for $\Delta(m/q)/(m/q)$ if the isochronicity condition $\gamma = \gamma_{\rm tr}$ is fulfilled. An appropriate ion optical setting has been developed for $\gamma_{\rm tr} = 1.37$ [58] and its performance has been investigated with ion beams, whose mean momenta were modified with the electron cooler. As can be seen from figure 6, there is only a very weak dependence of the revolution time on the ion velocity: within the storage momentum acceptance of approximately $\Delta p/p \simeq 0.55\%$ the revolution time is affected by $\Delta T/T \simeq 0.01\%$ only.

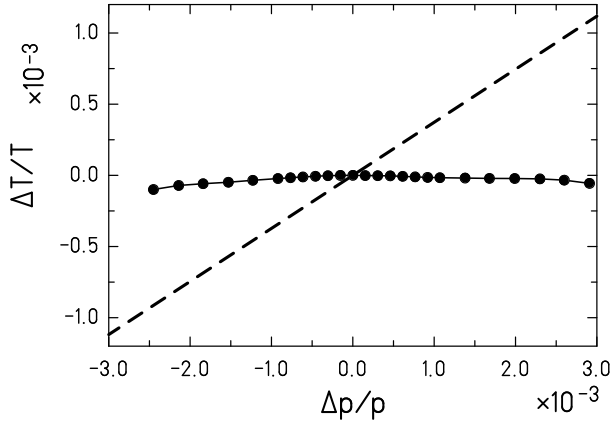

FIGURE 6. Relative change of revolution time $\Delta T/T$ versus relative momentum deviation $\Delta p/p$. The data points have been obtained with an isochronous ion-optical setting for $\gamma_t = 1.37$ with bare ^{58}Ni ions [58]. The dashed line shows the time-of-flight variation for the ESR standard ion optics ($\gamma_t \simeq 2.5$) for comparison.

For direct mass measurements of short-lived nuclei the revolution time T is obtained from a time-of-flight measurement of each turn for each individual ion. The measurements start with the injection into the ESR and the ions can be observed for typically 10 to 50 μs corresponding to approximately 20 to 100 turns of the ions before they are lost. The unknown masses are obtained from isotopes with known

masses by linear interpolation according to equation (2). Therefore the FRS must provide several different isotopes simultaneously, but a preselection of injected ions with the $B\rho$–ΔE–$B\rho$-separation method must be applied aiming at a balance of isotopes with known and unknown masses in order to avoid deadtime effects of the detection system due to those fragments with known masses which appear with high rates. In a recent experiment with fragments of a ^{52}Cr beam the masses of the neutron-deficient isotopes ^{41}Ti, ^{43,44}V, ^{45}Cr, and ^{48}Mn could be determined for the first time. A mass resolution of $m/\Delta m(\mathrm{FWHM}) = 1 \cdot 10^5$ and a mass accuracy of the order of 100 keV was achieved, for details and most recent results see ref. [59]. Although these nuclei have half-lives of the order of $T_{1/2} \sim 100$ms, the measurement time was of the order of 50μs or even less. Therefore, the same performance and accuracy is to be expected for nuclei with half-lives of the order of $T_{1/2} \sim 10\mu$s!
Those extremely short-lived isotopes can only be accessed with in-flight techniques and therefore unprecedented mass measurements are now possible with IMS. Moreover, new experiments aiming at the discovery and investigation of isomers are feasible now. Direct mass measurements with longer-lived nuclei are possible in the ESR with Schottky Mass Spectrometry.

Large-area mass determinations with Schottky Mass Spectrometry (SMS)

Another approach to cancel the second term in equation (2) is to minimize the relative velocity spread $\Delta v/v$ by means of electron cooling [22]. This technique is known as Schottky Mass Spectrometry [60,18] because the frequency determination is performed with Schottky diagnosis. So far, a mass-resolving power $m/\Delta m(\mathrm{FWHM}) \simeq 6.5 \cdot 10^5$ has been reached. Further improvements are expected from a still better stabilization of the ESR magnet power supplies, narrower temperature distributions of the cooling electrons, the new time-capture data acquisition [61], and the use of an ultra low noise resonant Schottky pickup cavity [62]. Schottky spectroscopy has no deadtime effects and hence it is desirable to inject many different isotopes simultaneously in order to get many correlations between isotopes with known and unknown masses at a time, therefore the FRS is operated as a pure magnetic-rigidity analyzer. SMS is presently the only experimental technique where a large mass surface can be mapped.
In experiments carried out so far with Bi primary beams more than 200 masses of neutron-deficient isotopes in the region from caesium to uranium, whose mass was unknown before [45], have been directly measured [16,63,64] with an accuracy of typically 100 keV. The lower limit of accessible half-lives lies around 5s due to the time necessary for cooling of the hot fragment beams and the time for measurement, which depends on the desired frequency bandwidth and frequency resolution and is of the order of few seconds to few minutes.
At the end of this section table 1 summarizes the main features and the performance of the experimental setups for direct mass measurements described in this paper. The experiments behind SHIP are described in the outlook.

TABLE 1. Characteristic features and parameters of the described experiments and techniques for direct mass measurements

	ISOLDE		SIS-FRS-ESR		SHIP	
production and separation	ISOL		fragmentation, ED, in-flight		heavy ion fusion, in-flight	
spectrometer	Penning trap	Smith type	storage ring		Penning trap	MR-TOF
mass range	$1 \leq A \leq 238$				$A \geq 238$	
accessible half-lives	$\geq$ 100ms	$\geq$ 1ms	$\geq$ 1s	$\geq 1\mu$s	$\geq$ 1s	$\geq 100\mu$s
cooling	buffer gas	no	electrons	no	buffer gas	no
mass resolving power $m/\Delta m$ (FWHM)	$6.0 \cdot 10^{5}$ [a]	$1.0 \cdot 10^{5}$ [b]	$6.5 \cdot 10^{5}$ [c]	$9.0 \cdot 10^{4}$ [d]	$10^{6} \ldots 10^{8}$ [e]	$\geq 10^{5}$ [e]
mass accuracy	15keV [a]	10 ... 20keV [b]	100keV [c]	100keV [d]	15keV [e]	50keV [e]

[a] for masses around $A = 130$ and an excitation time of 0.9s, the mass resolving power can become as high as $8.0 \cdot 10^{6}$ in this mass range using an excitation time of 12s [46]
[b] for masses around $A = 30$ [55]
[c] independent of mass [16,61]
[d] for masses around $A = 45$ [59]
[e] design goal

Exemplary results

In this section results obtained at the ISOLTRAP experiment and with SMS at the ESR will be presented and discussed. As some representative results the mass values obtained for the even-even barium and polonium isotopes are displayed in figure 7 in comparison with the predictions of different mass models. The Finite-Range

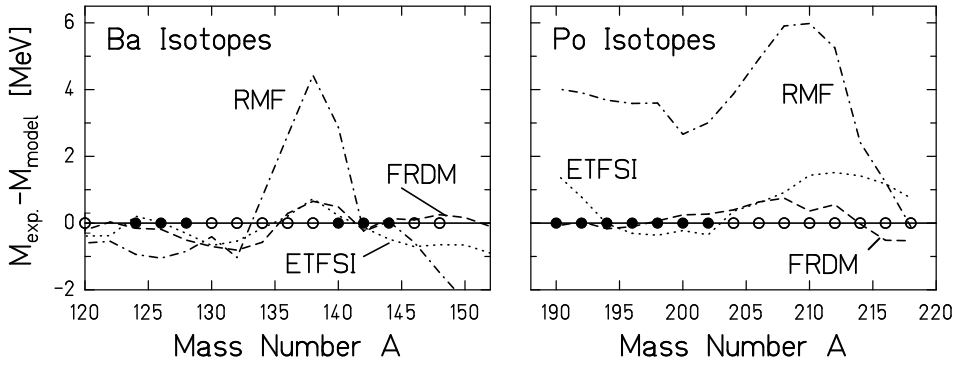

FIGURE 7. Comparison of experimental masses of even-A barium [46,45] (left panel) and polonium isotopes [64,45] (right panel) with the predictions of various nuclear models as indicated. The mass values obtained from the present experiments are shown with full dots while the previously known masses from ref. [45] are shown with open symbols.

Droplet Model (FRDM) [65] is a macroscopic-microscopic nuclear model where the macroscopic part accounts for the bulk contribution to the binding energy and the microscopic part accounts for shell and pairing effects. The Extended Thomas-Fermi model with Strutinski Integral (ETFSI) [66] combines the self-consistent Hartree-Fock approach with a shell correction term obtained using the Strutinski-integral

method. Therefore this model is in principle similar to the macroscopic-microscopic approach, but in ETFSI the two parts are connected much tighter because the same Skyrme-type force governs both parts. A fully microscopic model is the Relativistic Mean Field approach (RMF) [67], which yields ground-state properties of even-even nuclei such as binding energies, nuclear radii and deformation parameters. The effective force NL3, which has been fitted to ground-state properties of 10 spherical nuclei, is used to describe the effective nucleon-nucleon interaction. The best agreement between calculated and experimental masses is found for the macroscopic-microscopic FRDM, whereas the fully microscopic RMF calculation shows the largest discrepancies. However, it is important to note that the total binding energy of polonium isotopes is of the order of 1500 MeV and thus the RMF results are accurate to 0.3%.
In all mentioned calculations deformation is included. The phenomenon of deformation and shape coexistence is well established in the Pb region [68–70]. Recent studies within the framework of the Particle-Core Model (PCM) show that the interplay between spherical structures and an intruder band in the light polonium isotopes leads to strong deformations [71]. The ground state of ^{192}Po is expected to have oblate shape, whereas for still lighter Po isotopes prolate ground state shapes are predicted.
The experimental mass values can be used for the analysis of deformation and of the nuclear shell structure. A macroscopic-microscopic model has been fitted to the experimental mass values obtained for the barium isotopes and the deformation parameter β_2 revealing the quadrupole deformation of the nuclear potential has been extracted [46]. In the left panel of figure 8 the theoretical values are compared with data obtained from optical isotope shift measurements. Both sets of data clearly

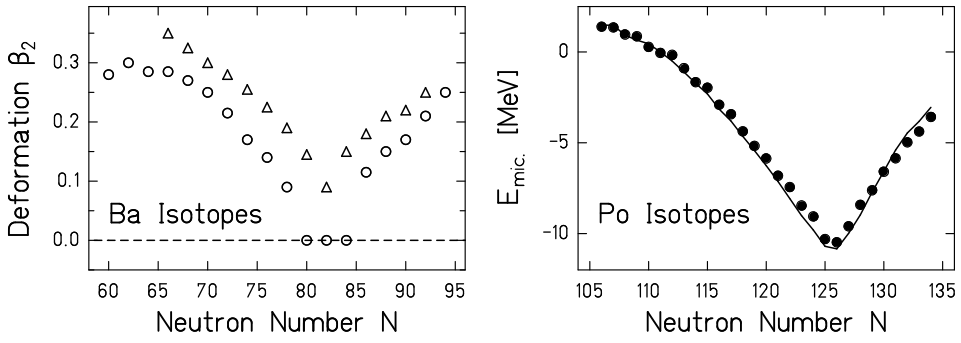

FIGURE 8. Shell structure effects explored with a macroscopic-microscopic model. The vanishing quadrupole deformation observed for barium isotopes [46] at $N = 82$ (left panel) and the pronounced minimum of microscopic energy [65] for polonium isotopes at $N = 126$ (right panel) clearly indicate the corresponding shell closure. The triangles in the left panel represent the result of isotope-shift measurements and the circles are calculation results (for details see [46]).

reveal the shell closure at the 'magic' neutron number $N = 82$ in terms of the vanishing deformation and show increasing prolate deformation for the lighter and for the heavier barium isotopes, respectively. The absolute values of both sets of data show fair agreement (for a more detailed discussion see [46]).

In the right panel of figure 8 the shell closure at ^{210}Po corresponding to the magic neutron number $N = 126$ is clearly seen from the microscopic part of the nuclear binding energy $E_{\mathrm{mic.}}$, which is defined as the experimental ground-state binding energy minus the macroscopic energy according to the FRDM [65]. Within the macroscopic-microscopic model the macroscopic liquid-drop term varies only smoothly with neutron number and the two major contributions to the microscopic energy are shell-correction energy and pairing energy. It has been pointed out earlier [72,73] that deformations set in at $A \simeq 199$ and the calculated potential-energy surface of polonium nuclei becomes shallow for $A \leq 194$.

Half-life measurements with highly-charged ions in the ESR

Pioneering experiments

With the combination of the fragment separator FRS [13] and the experimental storage ring ESR [15] it is for the first time possible to store exotic nuclei in a storage ring [74] and to investigate nuclear β-decay properties in selected ionic charge states. This offers the unique possibility to manipulate and to study nuclear half-lives in dependence of the number of attached electrons [75] and to study few-electron ions or bare nuclei under conditions which usually occur only in hot plasmas of a star where nucleosynthesis takes place [76,77]. With bare ions, where orbital electron capture (EC) is impossible, one can study or search for weak β^+-decay channels [78,79]. For instance it is a very important question for supernovae scenarios, whether there is a weak β^+-branch in the doubly-magic ^{56}Ni [80].
By inverting the time-arrow of orbital electron capture one comes back to a β^--decay, but with the created electron bound in an inner shell of the daughter atom, the 'bound-state β^--decay', β_b. Whereas this process represents only a scarce decay branch in neutral atoms because there are no inner-shell vacancies, it becomes the more important the higher the mother atom is ionized, as for instance in hot stellar plasmas. For those highly ionized atoms β_b-decay enhances the Q-value of the β-decay into the continuum, β_c, by approximately the binding energy of the created electron. To observe β_b-decay in a terrestrial laboratory one has to preserve a high ionic charge state for an extended period of time (of the order of hours) which is nowadays only possible in the ultra-high vacuum conditions in storage rings or ion traps. Hence, bound-state β-decay was experimentally observed for the very first time at the heavy ion storage ESR [81]. For this pilot experiment a striking example has been chosen: ^{163}Dy, which is stable as a neutral atom because the Q-value for continuum β-decay to ^{163}Ho is negative, $Q_{\beta_c} = -2.56$keV, might decay as a bare ion by β_b-decay to the ground state of ^{163}Ho with a positive Q-value of roughly 50keV for the electron being emitted into the K-shell of the daughter atom. This decay has indeed been observed and the measured half-life of (48^{+5}_{-4})d agrees nicely with the theoretically expected half-life of 50d [81].
In a second experiment β_b-decay of bare ^{187}Re has been investigated at the ESR [82]. The couple ^{187}Re/^{187}Os serves, together with the couple ^{238}U/^{232}Th, as a 'clock' for the age of our Milky Way galaxy, due to the half-life of $42 \cdot 10^9$yr for the neutral ^{187}Re

atom. However, for bare $^{187}Re^{86+}$ the experiment yielded a half-life dramatically reduced by nine orders of magnitude of only (33 ± 2)yr, due to an open β_b-decay channel to the first excited state of ^{187}Os at 10keV excitation energy, which is not accessible for neutral ^{187}Re [82]. In this case, the nuclear matrix element, the ft-value, for the transition to the excited osmium state was experimentally not known before, in contrast to the dysprosium experiment where the corresponding ft-value could be determined from the measured half-life of the orbital EC-decay of the ground state of neutral ^{163}Ho into the ground state of ^{163}Dy. This crucial dependence of the β-half-life on the ionic charge state shows that the Re/Os-couple and also other eon clocks based on long-lived radioactive nuclides can provide constraints for the age of our galaxy only within a detailed and reliable model of the history of nucleosynthesis and chemical evolution of stars [83]. That means that those 'nuclear' clocks are, basically, on the same footing as the well-known 'astronomical' clocks like globular clusters, white dwarfs etc., which also have to be 'calibrated' by the time scale of stellar evolution. The hope that radioactive nuclear couples could serve as clocks, independent of the widely unknown galactic history, has to be withdrawn.

Future experiments exploring weak-interaction decays

A forthcoming experiment concerning bound-state β-decay will address the couple ^{205}Tl/^{205}Pb [84]. Neutral ^{205}Pb decays to the ground state of ^{205}Tl by orbital electron capture with a half-life of $1.5 \cdot 10^7$yr and a Q-value of about 50keV. The ^{205}Tl nucleus, on the other hand, can be transformed to the first excited state of ^{205}Pb at 2.3keV excitation energy by capturing solar neutrinos from the pp-cycle ($E_{\max} =$ 420keV). Therefore, the relative ^{205}Tl/^{205}Pb abundance in deep-lying, thallium-rich ore bodies provides, when corrected for background, the product of the solar pp-neutrino flux, averaged over the lifetime of the ore bodies, and of the pp-neutrino capture probability into the 2.3keV state of ^{205}Pb, which is the dominant capture channel for pp-neutrinos. In this respect, ^{205}Tl serves as an integrating solar pp-neutrino detector like ^{71}Ga does in the GALLEX and SAGE experiments, but with two significant differences: the threshold for the pp-neutrino energy is much lower (50keV as compared to 235keV for ^{71}Ga) and the integration time of the solar neutrino flux is quite different (typical lifetime of the ore bodies of some million years as compared to a few days in the ^{71}Ga experiments). Now, for bare or hydrogen-like ^{205}Tl bound-state β-decay into ^{205}Pb becomes energetically allowed with a positive Q-value of about 40keV for the bound electron being in the K-shell of ^{205}Pb. Since the ground state of ^{205}Tl, ground state of ^{205}Pb and 2.3keV state of ^{205}Pb have the spins $I = 1/2^+$, $5/2^-$, and $1/2^-$, respectively, and since the second excited state of ^{205}Pb is as high as 263keV ($I = 5/2^-$), β_b-decay from the ^{205}Tl ground state feeds practically exclusively the 2.3keV level of ^{205}Pb, as it is the case for the capture of pp-neutrinos. The only way to determine precisely and reliably the unknown nuclear matrix element for this transition and, hence, the solar pp-neutrino capture probability into this state, is a measurement of the half-life of bare or hydrogen-like ^{205}Tl (as proposed by P. Kienle [85]), from which the ft-value can be simply extracted. Systematics of near-lying nuclear levels with similar shell structure

gives as a very rough half-life estimate of about 1 year for bare ^{205}Tl. Hence, an experimental determination of the half-life of bare ^{205}Tl in the ESR should be even more simple than in the case of ^{187}Re with a half-life of 33 years.
In a next step we plan to measure for interesting cases β-lifetimes for well-defined ionic charge states, by adding or removing a certain number of electrons in the atomic cloud. Within some constraints, the charge state of heavy ions can be chosen arbitrarily and in this way the weak interaction decays can be influenced. The general behavior of the EC/β^+-branching ratio for bare, H-like, and He-like nuclei with atomic number $Z = 82$ is shown in figure 9. For a given Z and a fixed charge state the EC/β^+-branching ratio depends only on the $Q_{\rm EC}$-value, which is connected with the β^+-endpoint energy $E_{\rm max}$ by $Q_{\rm EC} = E_{\rm max} + 2 \cdot m_e c^2$, where $m_e c^2$ is the electron rest mass.

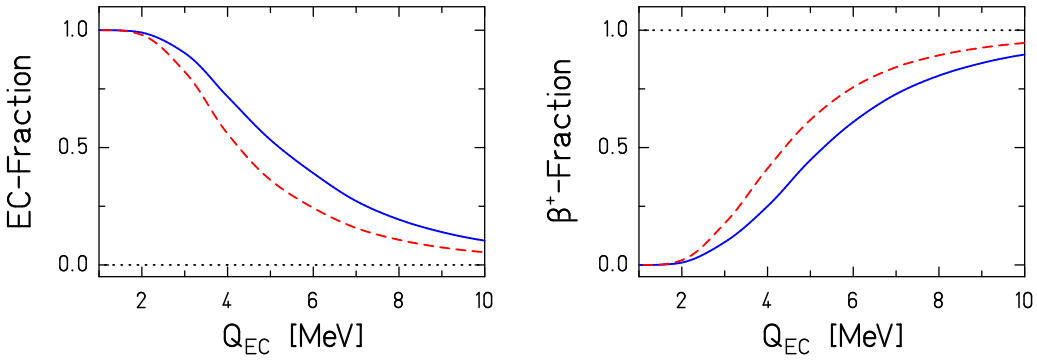

FIGURE 9. Branching ratio for EC and β^+-decay as a function of the $Q_{\rm EC}$-value. The figure shows the EC probability (left panel) and the β^+-decay probability (right panel) calculated according to ref. [86] for bare (dotted lines), hydrogen-like (dashed lines), and helium-like nuclei (solid lines) with atomic number $Z = 82$.

An other effect, which has been known theoretically for a long time [87], but which could not be confirmed experimentally, can now be investigated at the ESR: the influence of screening of the atomic electrons on the β-decay functions. Not only the low-energy part of β-ray spectra is influenced by the screening of the nuclear charge by atomic electrons but also the β-decay constant λ_β. The origin of this modification is a rather simple one, namely that λ_β is proportional to the integrated Fermi-function, that function which has been introduced by Fermi to account for the interaction between the Coulomb field and the emitted β-particles. The presence or absence of shell electrons modifies the Coulomb field of the nucleus and for a calculation of the screening effect it is therefore necessary to correct the wave function of the β-particle at the origin for the modified Coulomb field [86–89]. The screening effect increases with atomic number Z and with decreasing Q-value. It is very weak for β^--decay and much stronger for β^+-decay. In figure 10 the ratio $B = \lambda^*_\beta/\lambda_\beta$, is shown as a function of the β-endpoint energy $E_{\rm max}$ for $Z = 82$ for electrons (left) and for positrons (right) for $Z = 36$ (dashed line) and for $Z = 82$ (solid line). Here, λ^*_β denotes the β-decay-constant with screening and λ_β denotes the same quantity without screening. Thus, the ratio B is equal to the ratio of the integrated Fermi-

function with screening and the integrated Fermi-function without screening, which can be found in ref. [86].

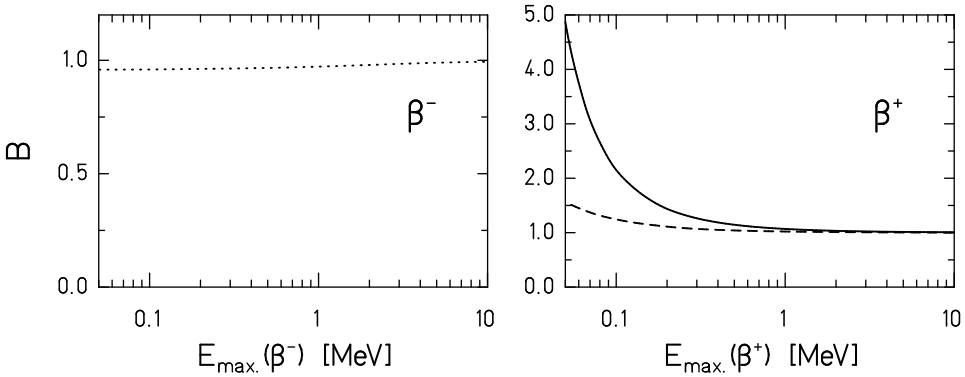

FIGURE 10. Screening effect depicted in terms of the ratio B (see text) as a function of the β-endpoint energy $E_{\max}(\beta)$. **Left:** β^--decay of a $Z = 82$-nucleus. **Right:** β^+-decay for $Z = 36$ (dashed line) and for $Z = 82$ (solid line). Note the different scales of the ordinate!

Schottky spectroscopy at the ESR is tailor-made for systematic and detailed investigations of the Fermi function in β-decay, for several reasons:

1. β-unstable ions in a well-defined ionic charge state carrying $0, 1, 2, \ldots$ electrons can be produced and separated with the FRS and injected, cooled and stored in the ESR for a long time.

2. Both, the mother- and daughter atom appear separated in the Schottky spectrum and can be unambiguously identified by their specific fingerprint. This is obvious for the common β^- and β^+-decay, where the ionic charge state will be changed by the decay. Moreover, it is even possible for EC- and β_b-decay where the ionic charge state does not change, if the corresponding Schottky lines are resolved, i. e., if the Q-value is sufficiently high. That supposes a Q-value exceeding a few hundred keV only (in the cases of ^{163}Dy and ^{187}Re discussed above the Q-values were only about 50keV and, thus, a more complicated detection method had to be applied, cf. refs. [81,82].

3. From the Schottky signals the number of the corresponding atoms can be determined as a function of time which provides the β-lifetime. The unique feature, that both, mother- and daughter atoms, can be counted simultaneously but independently at all times, improves significantly the accuracy in the lifetime evaluation.

From the ratio of the β_b-decay probability $\lambda_{\beta_b}(n)$ (resp. EC-decay probability $\lambda_{\rm EC}(n)$) into (resp. from) a well-defined state n of the bound electron and of the corresponding continuum decay probability λ_{β_c} of the neutral atom (resp. β^+-continuum decay probability λ_{β^+}) according to Bahcall [90] one gets immediately and independent of the nuclear matrix element, which drops out in this comparison, the ratio of the electron wave function in the final (resp. initial) state $\Psi_n(R)$ at the nuclear surface R and the Fermi function $f(Z, W_0)$

$$\lambda_{\beta_b}(n)/\lambda_{\beta_c} = \lambda_{\mathrm{EC}}(n)/\lambda_{\beta^+} = n_f \cdot Q_n^2 \cdot |\Psi_n(R)|^2/f(Z, W_0) \quad (3)$$

where n_f is the number of free (resp. occupied) places in the electron shell, Q_n the corresponding Q-value, Z the nuclear charge of the daughter (resp. mother) atom and W_0 the nuclear energy release in units of the electron rest energy for the corresponding continuum decay. Two regimes seem to be most interesting for this comparison:

1. concerning EC/β^+: the region just below and above the β^+-threshold, where the Q_{EC}-value is near $2m_ec^2$. Here, the Fermi function has by far the strongest dependence on Q_{EC}. A comparison of precisely measured decay probabilities of bare (pure β^+), hydrogen- and helium-like atoms could provide subtle and completely new information on both, the Fermi function and the density of the 1s electron wave function at the origin.
2. concerning β_b/β_c: bound-β decay of bare nuclei mainly into the K-shell. Most promising for this purpose are the nuclides ^{206,207}Tl and ^{205,206}Hg because of several reasons: the Q-values are in all cases about 1.5MeV, a separation of the Schottky lines for mother- and bound-beta daughter atoms, respectively, seems to be feasible. For those rather small Q-values and high atomic numbers $Z = 81, 80$ one expects a very strong β_b-branch to the K-shell, of the order of 20% to 30% of the total β-decay probability. Finally, those high Z and small Q-values are most sensitive probes for the 1s electron wave function as well as for the Fermi function.

OUTLOOK AND CONCLUSIONS

After the first generation of experiments with exotic nuclei at storage rings and ion traps new experimental facilities are coming up like the already mentioned AD experiments [1] and the HITRAP [32] project. At both facilities the ions are decelerated in storage rings and then captured, bunched, cooled and finally trapped. However, when one wants to investigate nuclei far off stability with very short half-lives, say below milliseconds, which can be investigated at in-flight separators exclusively, it is necessary to develop new schemes for deceleration and new investigation methods, which are fast and highly efficient. The fastest way of deceleration is the slowing down in matter, which brings even relativistic heavy ions to rest in time spans less than one nanosecond [91]. Schemes, where a fragment separator or a recoil separator is coupled to a stopping and bunching unit (which is similar to an IGISOL-type gas cell), are presently under discussion in many laboratories and are a new way to experiments with isotopically clean low-energy secondary beams with sub-millisecond half-lives. These fast deceleration schemes are completed by new fast and sensitive methods for measurements.

Here, we want to propose a new system for deceleration of heavy exotic nuclear beams combined with a new device for sub-millisecond direct mass measurements. Figure 11 shows a schematic view of the system, which consists of three main parts: a dispersive ion-optical system for fast slowing down and range bunching, a gas-filled stopper cell with an extraction, cooling, and bunching unit, and a multi-reflection

time-of-flight mass spectrometer. The whole system can be coupled to an in-flight separator. In the first unit, the separated swift exotic nuclear beams are slowed down and range bunched taking advantage of the combination of a dispersive dipole stage (3QD3Q2Q) with the slowing down in homogeneous and wedge-shaped degraders [91]. The beam is then stopped in a gas cell, extracted and cooled and bunched in a gas-filled quadrupole [92]. Then the pulse of low-energy monoisotopic

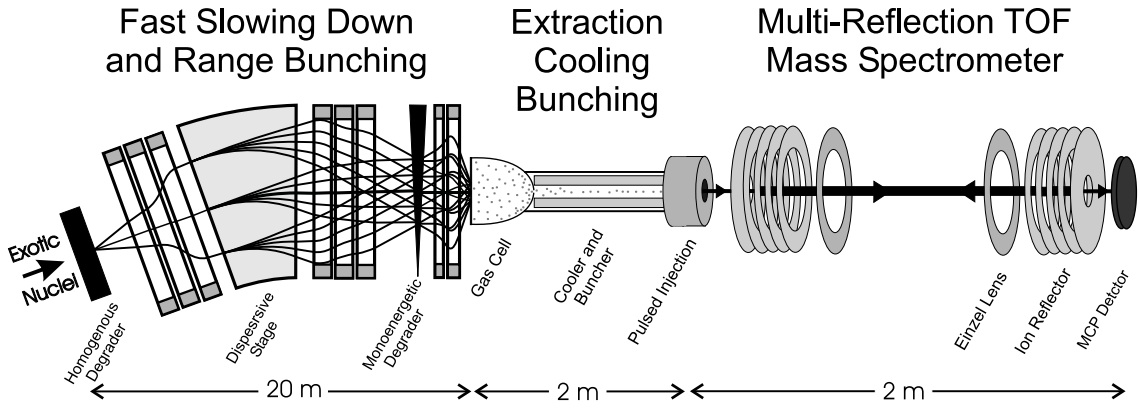

FIGURE 11. Schematic view (not to scale!) of a setup for sub-millisecond direct mass measurements with monoisotopic exotic nuclei showing the three main components for 1) fast slowing down and range bunching [91], 2) extraction, cooling, and bunching [92], and 3) direct mass measurements [93].

exotic nuclei is injected into an energy-isochronous multi-reflection time-of-flight mass analyzer [93] for direct mass measurements. These 'table-top' devices, in which ions are reflected back and forth between two or more electrostatic ion mirrors are presently under development for spectroscopic investigations at extraterrestrial sites, for instance for the exploration of the surface composition of comets [94]. The mass determination with such a spectrometer is based on the time-of-flight measurement of ions with keV energies in a given pathlength. In order to reach a high mass resolving power, which is proportional to the pathlength, the ions are multiply reflected between electrostatic grid-free ion mirrors before their arrival time is detected with a micro-channel-plate detector. The ion motion is achromatic and to second order energy isochronous and therefore the time-of-flight is directly proportional to the ions mass. Figure 12 shows the separated mass doublet CO^+-N_2^+ after 31 reflections in a one meter long spectrometer. A mass resolving power $m/\Delta m(\mathrm{FWHM}) = 51000$ is achieved after a measurement time as short as 724μs. As can be seen from the right part of the figure, the mass resolving power is directly proportional to the number of reflections or the measurement time. Without the data acquisition and analysis system being optimized for this purpose, a mass accuracy of 1ppm (corresponding to a mass uncertainty of 50keV for an $A = 50$-ion) has been reached with such a spectrometer [95]. Present limitations are due to power-supply instabilities ($\Delta U/U \simeq 5 \cdot 10^{-5}$) and the size of the initial phase space. For longer-lived species the mass resolving power can be increased by a longer flight time, either by increasing the number of reflections or by increasing the pathlength between the mirrors.

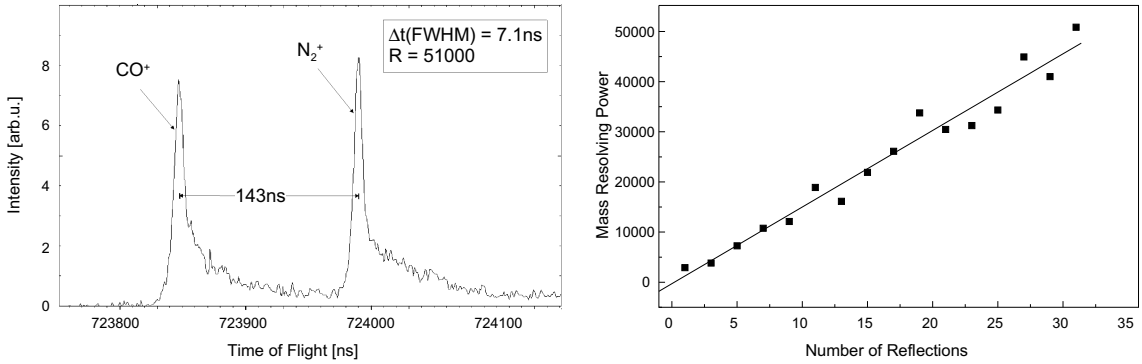

FIGURE 12. Left: part of a time-of-flight spectrum showing the mass doublet of N_2–CO after 31 passages through the one meter long multi-reflection time-of-flight mass spectrometer. **Right:** The mass resolving power increases quasi linearly with the number of reflections [94].

Also higher kinetic energies (presently $1.5 \cdot qe$ kV) and higher ionic charge states can lead to an increased mass resolving power. From this point of view multi-reflection time-of-flight mass spectrometers have a good potential for sub-millisecond mass measurements and will ideally complement the Penning trap mass measurements at the planned SHIPTRAP facility [31], which are better suited for longer-lived isotopes. The SHIPTRAP facility, which is designed also for other experiments with transuranium elements such as chemistry, optical spectroscopy, nuclear reaction studies, and nuclear spectrometry, will yield important experimental mass data which have been awaited for long time in the field of superheavy element research. The key parameter is the amount of microscopic energy which stabilizes superheavy elements (SHE). Experimental masses will allow a decisive determination of the location and strength of nuclear shells in SHE and are stringent tests of existing mass models. The data are also important for the prediction of reaction Q-values, the precise knowledge of which is crucial for SHE production, because systematic studies of cold-fusion reactions at SHIP have shown that the window of excitation energies becomes steadily narrower when going to heavier and heavier elements.

Finally it should be noted that there are also other possible applications for a multi-reflection time-of-flight spectrometer: 1) It can be used as a fast isobar separator: when the extraction potential is applied for a short time interval, only those ions with the proper flight time, i. e., with the proper mass or mass range, respectively, are extracted. 2) if the loss rate of the ions can be minimized one can use these devices as storage devices and, e. g., for the transport of antiprotons [96]. The practical advantages are low weight of few kilograms only, small size, and little power consumption (note that multi-reflection time-of-flight mass spectrometers are adapted to the needs of space missions).

In conclusion, storage rings and ion traps are facilities which are well suited for the investigation of gross properties of exotic nuclei. Presently several different and complementary experimental setups are in operation, which provide important nuclear structure data of short-lived nuclei far-off stability, a field living vividly from the interplay of experiment and theory. Schottky Mass Spectrometry with stored cooled

ions is capable of mapping large sectors of the mass surface, Penning trap measurements yield the most accurate mass values and time-of-flight techniques give access to the shortest-lived nuclei. Besides the mass values themselves the experimental results allow the study of shell effects, deformation, and decay properties at the limits of stability. The coming experiments at GSI will focus on mass measurements with fission products stored in the ESR and with fusion-reaction products at SHIP. Unprecedented half-life measurements with bare and few-electron ions will lead to new insights into β-decay. The next experiments have the potential to obtain new information on the Fermi function, the density of the 1s electron wave function at the origin, and the role of electron-electron correlations.

ACKNOWLEDGEMENTS

For fruitful and stimulating discussions we are full of gratitude to G. Audi, M. Hausmann, F. Herfurth, O. Klepper, H.-J. Kluge, C. Kozhuharov, M. D. Lunney, C. Monsanglant, Yu. N. Novikov, T. Radon, M. de Saint Simon, J. Stadlmann, H. Schatz, S. Schwarz, and C. Thibault. One of us (C. S.) would like to thank CERN and the ISOLDE collaboration for a one-year Scientific Associateship and the MISTRAL and the ISOLTRAP groups for their hospitality during the stay.

REFERENCES

1. J. Eades, F. J. Hartmann, *Rev. Mod. Phys.* **71** (1999) 373.
2. S. Peil, G. Gabrielse, *Phys. Rev. Lett.* **83** (1999) 1287.
3. B. Jonson, A. Richter, accepted for publication in *Hyp. Int.*
4. H. Geissel *et al.*, *Annu. Rev. Nucl. Part. Sci.* **45** (1995) 163.
5. C. Détraz, D. J. Vieira, *Annu. Rev. Nucl. Part. Sci.* **39** (1989) 407.
6. H. Ravn, *Phil. Trans. R. Soc. Lond.* **A356** (1998) 1955.
7. For an overview see: *Proceedings of Stori 1996*, eds. F. Bosch and P. Egelhof, *Nucl. Phys.* **A626** (1997).
8. G. Münzenberg, *Nucl. Instr. Meth.* **B70** (1992) 265.
9. G. Münzenberg *et al.*, *Nucl. Instr. Meth.* **161** (1979) 65.
10. V. Ninov *et al.*, *Nucl. Instr. Meth.* **A357** (1995) 486.
11. T. S. Nikolaev, T. S. Dimitriev, *Sov. Phys. Tech. Phys.* **15** (1971) 1383.
12. N. Bohr, *K. Dan. Vidensk. Selsk. Mat. Fys. Medd.* **18(8)** (1948).
13. H. Geissel *et al.*, *Nucl. Instr. Meth.* **B70** (1992) 286.
14. C. Scheidenberger *et al.*, *Nucl. Instr. Meth.* **B142** (1998) 441.
15. B. Franzke *et al.*, *Nucl. Instr. Meth.* **B24/25** (1987) 18.
16. H. Geissel *et al.* in *Proceedings of the 2nd International Conference on Exotic Nuclei and Atomic Masses (ENAM98)*, Bellaire, Michigan, USA.
17. J. Borer *et al.*, *Proceedings IXth Conf. High Energy Accelerators*, Stanford (1974) 53.
18. B. Schlitt *et al.*, *Hyp. Int.* **99** (1996) 117.
19. B. Franzke *et al.*, *GSI Scientific Report 1995* **GSI96-1** (1996) 159.
20. F. Nolden*et al.*, *Nucl. Phys.* **A626** (1997) 491c.
21. M. Steck *et al.*, *Phys. Rev. Lett.* **77** (1996) 3803.
22. M. Steck *et al.*, *Nucl. Phys.* **A626** (1997) 495c.
23. H. L. Ravn *et al.*, *Nucl. Instr. Meth.* **B126** (1997) 176.

24. R. B. Moore *et al.*, *Physica Scripta* **T59** (1995) 93, and
W. M. Itano *et al.*, *ibid.*, 106.
25. H.-J. Kluge *et al.*, in *Proceedings of the International Conference on Nuclear Shapes and Nuclear Structure at Low Excitation Energies*, eds. M. Vergnes, D. Goutte, P. H. Heenen, J. Sauvage, Antibes (1994) 83.
26. G. Bollen *et al.*, *Nucl. Instr. Meth.* **A368** (1996) 675.
27. M. König *et al.*, *Int. J. Mass Spectrom. Ion Processes* **142** (1995) 95.
28. H. Raimbault-Hartmann *et al.*, *Nucl. Instr. Meth.* **B126** (1997) 378.
29. G. Savard *et al.*, *Phys. Lett.* **A158** (1991) 247.
30. D. Habs *et al.*, *Nucl. Instr. Meth.* **B139** (1998) 128.
31. Latest news on SHIPTRAP can be found in the World Wide Web at the following site: `http://www-aix.gsi.de/~shiptrap/`
32. M. Diederich *et al.*, *Phys. Scripta* **T80** (1999) 437. More information about the HITRAP project is available from `http://www-aix.gsi.de/~eurotrap/hitrap.htm`
33. W. Quint, *Physica Scripta* **T59** (1995) 203, and
G. Werth, *ibid.*, 206.
34. M. H. Holzscheiter *et al.*, Proposal SPSLC96-47/P302, presented to the CERN SPSLC on 20. October 1996, available from `http://www.cern.ch/~athena/`
35. G. Gabrielse *et al.*, Proposal SPSLC97-8/P306, presented to the CERN SPSLC on 25. March 1997, available from `http://hussle.harvard.edu/~atrap/`
36. G. Gabrielse *et al.*, *Phys. Rev. Lett.* **82** (1999) 3198.
37. G. Bollen, *Nucl. Phys.* **A626** (1997) 297c.
38. W. Mittig *et al.*, *Annu. Rev. Nucl. Sci.* **47** (1997) 27.
39. W. Nazarewicz *et al.*, *Phys. Scripta* **T56** (1995) 9.
40. J. B. Ehrman, *Phys. Rev.* **81** (1951) 412.
41. R. G. Thomas, *Phys. Rev.* **88** (1952) 1109.
42. S. Aoyama *et al.*, *Phys. Rev.* **C57** (1998) 975.
43. E. P. Wigner, *Phys. Rev.* **51** (1937) 106.
44. P. Van Isacker *et al.*, *Phys. Rev. Lett.* **74** (1995) 4607.
45. G. Audi, *et al.*, *Nucl. Phys.* **A624** (1997) 1.
46. F. Ames *et al.*, *Nucl. Phys.* **A651** (1999) 3.
47. E. G. Adelberger *et al.*, *Phys. Rev. Lett.* **83** (1999) 1299, and
Phys. Rev. Lett. **83** (1999) 3101.
48. J. Deutsch, P. Quin, in *Precision Tests of the Standard Electroweak Model* (ed. Paul Langacker, World Scientific, Singapure, 1993).
49. M. S. Antony *et al.*, *At. Data Nucl. Data Tables* **33** (1985) 447.
50. M. D. Lunney *et al.*, *Hyp. Int.* **99** (1996) 105, and
M. D. Lunney *et al.* in *Proceedings of the 2nd International Conference on Exotic Nuclei and Atomic Masses (ENAM98)*, Bellaire, Michigan, USA.
51. J. Trötscher *et al.*, *Nucl. Instr. Meth.* **B70** (1992) 455.
52. L. G. Smith, *Proc. 3rd Int. Conf. on Atomic Masses*, University of Manitoba Press, Winnipeg (1967) 811.
53. M. de Saint Simon *et al.*, *Nucl. Instr. Meth.* **B70** (1992) 459.
54. C. Toader *et al.*, in *Proceedings of the International Conference on Trapped Charged Particles and Fundamental Physics*, Asilomar, AIP Conf. Proc. 457, eds. Daniel H. E. Dubin, Dieter Schneider (1999) 95.
55. C. Monsanglant *et al.*, accepted for publication in *Proceedings of the International*

Conference on Experimental Nuclear Physics Facing the Next Millenium, Seville (1999).
56. J. M. Wouters *et al.*, *Nucl. Instr. Meth.* **B26** (1987) 286.
57. H. Wollnik *et al.*, *Nucl. Phys.* **A626** (1997) 327c.
58. M. Hausmann, doctoral thesis, Justus-Liebig-Universität Gießen (1999), and M. Hausmann *et al.*, accepted for publication in *Nucl. Instr. Meth.* **A**.
59. J. Stadlmann *et al.*, contribution to this conference.
60. B. Franzke *et al.*, *Physica Scripta* **T59** (1995) 176.
61. M. Falch *et al.*, contribution to this conference.
62. C. Gonzalez, F. Pedersen, *Proceedings Particle Accelerator Conference 1999*, New York (1999), 474.
63. T. Radon *et al.*, *Phys. Rev. Lett.* **78** (1997) 4701.
64. T. Radon *et al.*, submitted for publication in *Nucl. Phys.* **A**.
65. P. Möller *et al.*, *At. Data Nucl. Data Tab.* **59** (1995) 185.
66. Y. Aboussir, J. M. Pearson, *At. Data Nucl. Data Tab.* **61** (1995) 127.
67. G. A. Lalazissis *et al.*, *At. Data Nucl. Data Tab.* **71** (1999) 1.
68. G. Ulm *et al.*, *Z. Phys.* **A325** (1986) 247.
69. M. P. Carpenter *et al.*, *Phys. Rev. Lett.* **78** (1997) 3650.
70. W. Nazarewicz, *Phys. Lett.* **B305** (1993) 195.
71. A. M. Oros *et al.*, *Nucl. Phys.* **A645** (1999) 107.
72. I. Ragnarsson *et al.*, *Physica Scripta* **29** (1984) 385.
73. R. Bengtsson *et al.*, *Physica Scripta* **29** (1984) 402.
74. H. Geissel *et al.*, *Phys. Rev. Lett.* **68** (1992) 3412.
75. F. Bosch, *Physica Scripta* **T59** (1995) 221.
76. D. D. Clayton, *Astrophys. J.* **139** (1964) 637.
77. K. Takahashi, K. Yokoi, *Nucl. Phys.* **A404** (1983) 578.
78. H. Irnich *et al.*, *Phys. Rev. Lett.* **75** (1995) 4182.
79. O. Klepper, *Nucl. Phys.* **A626** (1997) 119c.
80. D. D. Clayton, *Principles of stellar evolution and nucleosynthesis*, McGraw-Hill Book Company, New York, 1968.
81. M. Jung *et al. Phys. Rev. Lett.* **69** (1992) 2164.
82. F. Bosch *et al.*, *Phys. Rev. Lett.* **77** (1996) 5190.
83. F. Bosch, *Phys. Scripta* **T80A** (1999) 28.
84. M. S. Freedman *et al.*, *Science* **193** (1976) 1117, and M. S. Freedman, *Nucl. Instr. Meth.* **A271** (1988) 267.
85. P. Kienle, *Nucl. Instr. Meth.* **A271** (1988) 277.
86. H. Behrens, J. Jänecke, *Numerische Tabellen für beta-Zerfall und Elektronen-Einfang* (ed. H. Schopper, Springer Verlag, Berlin, 1969).
87. M. E. Rose, *Phys. Rev.* **49** (1936) 727.
88. W. Bühring, *Nucl. Phys.* **61** (1965) 110.
89. B. Crasemann, *Nucl. Instr. Meth.* **112** (1973) 33.
90. J. N. Bahcall, *Phys. Rev.* **124** (1961) 495.
91. H. Weick *et al.*, accepted for publication in *Nucl. Instr. Meth.* **B**.
92. G. Bollen *et al.* in *Proceedings of the 2nd International Conference on Exotic Nuclei and Atomic Masses (ENAM98)*, Bellaire, Michigan, USA.
93. H. Wollnik in *AIP Conf. Nuclear Structure, Gatlinburg*, Proc. **184**, ed. C. Baktash (1999).

94. A. Casares *et al.*, in *Proceeding of the 47th ASMS Conference on Mass Spectrometry and Allied Topics, Dallas* (1999).
95. A. Casares, H. Wollnik, private communication (1999).
96. C. H. Tseng, G. Gabrielse, *Hyp. Int.* **76** (1993) 381.